ELSEVIER

Advances in Water Resources 24 (2001) 1051–1067

Advances in Water Resources

www.elsevier.com/locate/advwatres

Spatio-temporal evolution and time-stable characteristics of soil moisture within remote sensing footprints with varying soil, slope, and vegetation

B.P. Mohanty *, T.H. Skaggs

George E. Brown Salinity Laboratory, USDA-ARS, 450 W. Big Springs Road, Riverside, CA 92507, USA

Received 7 July 2000; received in revised form 26 January 2001; accepted 2 February 2001

Abstract

Air-borne passive microwave remote sensors measure soil moisture at the footprint scale, a scale of several hundred square meters or kilometers that encompasses different characteristic combinations of soil, topography, vegetation, and climate. Studies of within-footprint variability of soil moisture are needed to determine the factors governing hydrologic processes and their relative importance, as well as to test the efficacy of remote sensors. Gridded ground-based impedance probe water content data and aircraft-mounted Electronically Scanned Thinned Array Radiometer (ESTAR) pixel-average soil moisture data were used to investigate the spatio-temporal evolution and time-stable characteristics of soil moisture in three selected (LW03, LW13, LW21) footprints from the Southern Great Plains 1997 (SGP97) Hydrology Experiment. Better time-stable features were observed within a footprint containing sandy loam soil than within two pixels containing silty loam soil. Additionally, flat topography with split wheat/grass land cover produced the largest spatio-temporal variability and the least time stability in soil moisture patterns. A comparison of ground-based and remote sensing data showed that ESTAR footprint-average soil moisture was well calibrated for the LW03 pixel with sandy loam soil, rolling topography, and pasture land cover, but improved calibration is warranted for the LW13 (silty loam soil, rolling topography, pasture land) and LW21 (silty loam soil, flat topography, split vegetation of wheat and grass land with tillage practice) pixels. Footprint-scale variability and associated nonlinear soil moisture dynamics may prove to be critical in the regional-scale hydroclimatic models.

1. Introduction

Soil moisture is the natural state variable of the land surface. Its temporal and spatial variability over catchment areas affects surface and subsurface runoff, modulates evaporation and transpiration, determines the extent of groundwater recharge, and initiates or sustains feedback between the land surface and the atmosphere [31]. At a particular point in time soil moisture content is influenced by: (1) the precipitation history, (2) the texture of the soil, which determines the water-holding capacity, (3) the slope of the land surface, which affects runoff and infiltration, and (4) the vegetation and land cover, which influences evapotranspiration and deep percolation. To date very few studies have been made to quantitatively understand the multi-scale dynamics of soil moisture in land-surface hydrologic systems. Traditionally, soil moisture spatial variability studies using ground-based point-scale (i.e., sampling area of cm^2) measurements are limited to small fields with uniform soil characteristics, topographic features, and vegetative conditions. Lately the use of various active and passive microwave remote sensors [15] has enhanced the capability to monitor soil moisture in large land areas (i.e., hundreds of square meters to thousands of square kilometers) encompassing various soil types (e.g., texture), topographic features (e.g., slope), vegetation, and climatic conditions. These remote sensing signals give some kind of average value over an area usually known as a footprint. For larger footprints, only predominant soil and vegetation types are used for calibration purposes. An inherent difficulty of remotely sensed soil moisture measurement is relating soil moisture variability at the scale of the footprint to larger or smaller scale soil moisture variability [40].

Traditionally footprint-scale soil moisture measurements have been used for regional-scale hydrologic or

* Corresponding author. Tel: +1-909-369-4852; fax: +1-909-342-4964.

E-mail address: bmohanty@ussl.ars.usda.gov (B.P. Mohanty).

0309-1708/01/$ - see front matter
PII: S0309-1708(01)00034-3

general circulation modeling (GCM) studies. In the recent past concern has been raised that footprint-scale measurements may be too crude for providing a good understanding of hydrologic systems at the subgrid (field, catchment, basin, watershed) scales. Hence errors at the level of catchments, basins, and watersheds may add up to providing inaccurate regional-scale hydroclimatic predictions by the GCMs. Njoku and Entekhabi [33] also suggested that the meaning of 'soil moisture' as an average quantity over a heterogenous volume, and its usefulness in a hydrologic sense, needs to be carefully examined. Charpentier and Groffman [6] discussed the limitations of soil moisture obtained by remote sensing techniques. They suggested that several factors such as vegetation, soil texture, surface roughness, and temperature of the upper surface layer affect the ability of the radiometers to measure thermal emissions from the soil. In addition to problems with environmental factors, remote sensing of soil moisture is complicated by within-pixel variability. Remote sensing devices give information only on the average moisture conditions within a pixel. Since remote sensors provide only one value per pixel, the extent of within-pixel variability affects how well the remotely sensed measure reflects moisture conditions within the pixel and thus affects the usefulness of remotely sensed data. For example, within-pixel variability is important when soil moisture data are needed to study biogeochemical processes such as trace gas fluxes. These processes are often very sensitive to extreme values of soil moisture and it is important to have an estimate of the distribution of values around the mean. Unless remote sensing techniques can provide some information on the occurrence of these extreme values, their usefulness will be limited.

Ground-based measurements and time-stability analysis within selected remote sensing footprints may help address some of these issues and result in general pattern(s) for the entire region. The time stability concept was introduced by Vachaud et al. [41] as the time-invariant association between spatial locations and classical statistical parametric values of soil properties. The concept appears especially promising for soil water behavior at the Earth's surface. Vachaud et al. [41] tested the concept on the measured water stored in a soil profile and suggested that time stability will occur if covariances exist between a spatial variable of interest and a deterministic factor such as soil texture or topography. Subsequent studies, including Kachanoski and de Jong [23], Kamgar et al. [24], and Grayson and Western [17], explored the time-stability idea for soil moisture persistence at various spatial scales. Kachanoski and de Jong [23] demonstrated that soil water storage at a point is the product of hydrologic processes at different spatial scales and that coherency analysis may be used to identify time stability features at these scales. Grayson and Western [17] explored the existence of certain parts of the landscape which consistently exhibit mean behavior irrespective of the overall wetness while other parts always represented extreme values. These studies concluded that the time-stability concept has potential for ground truthing large-scale remote sensing campaigns because reliable estimates of areal mean soil moisture in complex terrain could be obtained from a limited number of sampling locations. However, they suggested that the concept needs to be tested in a variety of places and over a large range of scales to determine whether there are definable features of soil, topography, vegetation, and climate that could be used to identify time-stable locations a priori.

In agricultural or pasture land, within-pixel variability of surface soil moisture is influenced by soil type, topography, vegetation, land management, and antecedent moisture. Variability in these factors in space and/or time can introduce systematic uncertainty into remotely sensed soil moisture data. However, if the factors controlling this variability can be determined and quantified, this uncertainty can be assessed. Moreover, it may be possible to use information on soil, topography, vegetation, antecedent moisture, and other factors to improve remotely sensed soil moisture data sets by adding estimates of uncertainty to the average values obtained by the remote sensor. In this study we investigated the time-stable features of surface soil moisture and the associated contributing factors at three selected footprints of an air-borne Electronically Scanned Thinned Array Radiometer (ESTAR) during the Southern Great Plains 1997 (SGP97) Hydrology Experiment in Oklahoma. We consider soil texture, slope, and vegetation type as distinguishable contributing factors for soil moisture variability within a footprint, and view meteorological conditions as a macroscale factor that is constant over each remote-sensing footprint (pixel). The specific objectives of this paper include: (1) monitoring the evolution of within-pixel spatial variability of daily soil moisture and related contributing factors in selected ESTAR footprints with different combinations of soil texture, slope, vegetation type, and precipitation events, and (2) examining the presence and causes of any time-stable ground monitoring locations within the selected ESTAR footprints.

2. Southern Great Plains 1997 (SGP97) Hydrology Experiment

The Southern Great Plains 1997 (SGP97) Hydrology Experiment was a coordinated collaborative effort by an interdisciplinary science team sponsored by the National Aeronautic and Space Administration (NASA), the US Department of Agriculture-Agricultural Research Service (USDA-ARS), the National Oceanic and

Atmospheric Administration (NOAA), the Department of Energy (DOE), the National Science Foundation (NSF), and other agencies. A detailed description of the experimental plan, including the different scientific objectives of the mission, can be found elsewhere http://hydrolab.arsusda.gov/sgp97/. The Southern Great Plains region in Oklahoma was selected for this experiment because it is one of the best-instrumented sites in the world for surface soil moisture, hydrology, and meteorology. A key objective of the SGP97 soil moisture team was to develop a good understanding of the spatio-temporal variability of soil moisture at a hierarchy of scales. During the SGP97 hydrology experiment (June 18–July 18, 1997), the soil moisture content was measured over an area greater than 10,000 km^2 at different resolutions using different platforms, including an aircraft-mounted L-band ESTAR measuring at a resolution of 800 m $\times$ 800 m, a truck-mounted microwave remote sensor measuring at a scale of 2.5 m $\times$ 2.5 m, and others.

A complete list of remote sensors used and their specifications can be found in the SGP97 experimental plan [http://hydrolab.arsusda.gov/sgp97/]. Concurrent to remote sensing, point-scale soil moisture measurements were made using (ground-based) gravimetric or electromagnetic techniques. At selected ESTAR footprints, a larger number of point measurements were made using impedance probes. Famiglietti et al. [13] presented the sample statistics of the extensive spatio-temporal soil moisture data for these footprints. A major finding of their study is that the range and temporal dynamics of the variability in moisture content between sites are consistent with variations in soil type, vegetation cover, and rainfall gradients. Mohanty et al. [28] adopted an intensive sampling scheme (800 measurements in 24 h within an area of 400 m$\times$ 160 m) and demonstrated several site-specific characteristics of soil moisture variability at a smaller field with uniform soil and vegetation and gently sloping topography. Their results indicated that moisture redistribution across the slope position was the most significant factor controlling the field-scale spatio-temporal variability of surface soil moisture. Furthermore, they concluded that among the hill-top, slope, and valley positions, sampling points on the slope render the most time instablility in the diurnal soil moisture distribution during a drying sequence.

3. Experimental design

The Little Washita watershed was a critical study area of SGP97. The watershed has been the focus of hydrologic research for over 35 years. The Little Washita watershed covers 610 km^2 and is a tributary of the Washita river in southwest Oklahoma. The watershed is in the southern part of the Great Plains of the US. The climate is classified as sub-humid with an average annual rainfall of 75 cm. The topography of the region is moderately rolling with a maximum relief of about 200 m. Soils include a wide range of textures with large areas of both coarse and fine textures. Rangeland and pasture with significant areas of winter wheat and other crops dominate land use. Additional background information on the watershed can be found in Allen and Naney [1] and Jackson and Schiebe [22].

We selected three (LW03, LW13, and LW21) 800 m $\times$ 800 m ESTAR footprints (pixels) for the present study. The geographic locations and other field attributes for these three fields are given in Table 1. The LW03 footprint is predominantly sandy loam with a few small patches of loam soil, gently rolling, rangeland field; LW13 is predominantly silty loam with a patch of loam soil, gently rolling, rangeland field; and LW21 is a silt loam, flat, split winter wheat/grass field. The LW21 pixel is located near the western edge of the Little Washita watershed, whereas LW03 and LW13 pixels are located in the north-central and eastern part of the watershed, respectively. During the SGP97 experiment LW03 and LW13 experienced a similar rainfall (temporal) pattern, which was somewhat different from that observed at LW21. Spatial variability of atmospheric variables within each pixel (800 m $\times$ 800 m) was neglected in this study. Based on the pixel-specific features, LW03 and LW13 differ mostly in terms of soil texture, LW13 and LW21 differ in terms of topography, vegetation, and precipitation, and LW03 and LW21 differ in soil texture, topography, vegetation, and precipitation. Thus differences in soil moisture dynamics among these pixels can be attributed to the respective factor(s) and any of their joint contribution(s). In this study, the claim of uniformity in soil properties related to soil moisture dynamics is based only on soil texture. While we acknowledge the general limitation of this assumption, it is noteworthy that there is a significant relationship between texture and soil hydraulic proper-

Table 1
Geographical locations and field attributes for LW03, LW13, and LW21 pixel

Pixel	Location UTM coordinates of the NE corner of the pixel	Soil texture SURRGO map	Land cover LANDSAT TM image and field obs.	Topography DEM
LW03	584467, 3869166	Sandy loam	Rangeland	Rolling
LW13	595701, 3864517	Silty loam	Rangeland	Rolling
LW21	566047, 3863463	Silty loam	Wheat/grass	Flat

ties [2,5,7,36]. The influence of soil texture on soil hydraulic and retention properties is particularly dominant in the mid to low soil water pressure range. On the other hand, bigger pores (soil structure) dominate the hydraulic properties near saturation. As mentioned below, we skipped sampling during heavy rainfall events, essentially limiting our data to the surface soil moisture regime that is dominated by soil texture, further justifying our assumption of uniform soil.

3.1. Remote sensing of soil moisture

An L-band passive microwave ESTAR instrument was used to measure the pixel-average daily surface (0–5 cm) soil moisture contents across the entire SGP97 region. For the sake of completeness we briefly describe the principles of microwave remote sensing and measurement of surface soil moisture content. More elaborate discussions on this topic can be found elsewhere [33,37]. A microwave radiometer measures the thermal emission from the surface and at these wavelengths the intensity of the observed radiation is proportional to the product of the thermodynamic temperature of the soil and the surface emissivity. This product is commonly called the brightness temperature. The soil emissivity at microwave wavelengths, about 1–30 cm, is a strong function of its moisture content because of the large dielectric contrast between dry soil ($\sim$3.5) and water ($\sim$80). The resulting emissivity for soil changes from about 0.95 for dry soil to about 0.6 for wet soils at a rate of approximately 0.01 per % volumetric moisture content. The rate is a function of the soil texture, being greater for lighter sandy soils and smaller for heavier clayey soils. The rate is also reduced by surface features, such as vegetation cover and roughness. For example, for a sufficiently thick layer of vegetation, only the radiation from the vegetation will be observed. Thus, to quantify the effect of vegetation on microwave emission from soils, it is necessary to have some estimate of above ground biomass for the plants. Similarly, higher soil surface roughness (microtopography) reduces its microwave reflectivity and thus increases its emissivity. Empirical models are generally used to adjust the remotely sensed soil moisture under varying degrees of surface roughness and vegetation cover.

To date no satellite-based L-band (21 cm wavelength) passive microwave system has been implemented for soil moisture monitoring. A few aircraft-based L-band microwave instruments (i.e., the push broom microwave radiometer (PBMR) and the ESTAR) have been developed and used in the past for mapping surface soil moisture [21] during watershed- or regional-scale hydrology campaigns. During the SGP97 field campaign, a NASA P-3 aircraft-based ESTAR instrument was used for daily soil moisture mapping across the 250 km $\times$ 60 km study region (Fig. 1). It is a synthetic aperture, passive microwave radiometer operating at a center frequency of 1.413 GHz and a bandwidth of 20 MHz. As installed it is horizontally polarized and integration time is 0.25 s. ESTAR flights were conducted at an altitude of about 7500 m. Overflights were suspended on a few days due to mechanical difficulties or unfavorable weather conditions. More specific details about the ESTAR instrument can be found at http://daac.gsfc.nasa.gov/CAMPAIGN_DOCS/ SGP97/estar.html.

3.2. Ground-based soil moisture measurement

For studying within-pixel variability of the three footprints, we designed a regular 7 $\times$ 7 square grid with 100-m spacings. The grid spacing was determined based on several factors: (1) available human and technical resources, (2) narrow time-window of daily sampling, and (3) prior research results in the same general region showing limited spatial structure of soil moisture at smaller lags [6,27]. Posterior analyses of SGP97 data sets also showed dominance of microheterogeneity [13,28]. Junction points were identified and flagged using a differential global positioning system (DGPS). The DGPS system was operated by using the correction signal transmitted by radio beacon from a reference station in Sallisaw, OK, which is part of a network maintained by the US Coast Guard. During the SGP97 hydrology campaign (June 18–July 18, 1997), the volumetric moisture content in the 0–6 cm surface soil layer was measured daily at the 49 (7 $\times$ 7) sampling points following a serpentine sequence for each of these fields. Two 2-person teams accomplished the daily sampling in 3–4 h each afternoon using two sets of portable impedance probes and DGPS units. Sampling was suspended during rain events or when agricultural activity posed a significant safety concern (cultivation on June 27 at LW21). In total, 23, 24, and 17 complete sets of daily soil moisture data were collected at LW03, LW13, and LW21, respectively.

The impedance probe used in the soil moisture measurements is a commercially available sensor (theta probe soil moisture sensor, type ML1, Delta-T Devices, Cambridge, England). This device measures soil moisture in the 0–6 cm soil layer, which closely matches the depth of ESTAR measurements (0–5 cm). The probe uses a simplified voltage standing wave method to determine the relative impedance of its sensing head (which consists of 4 sharpened, 6-cm long stainless steel wire rods), and thus the dielectric constant of the soil matrix, which is related to the volumetric water content of soil. Further details of the design and application of this technique can be found in Gaskin and Miller [14]. Calibration of this method around the SGP97 region by our collaborators indicated close agreement with the calibration curve of Gaskin and Miller [14]. Thus we

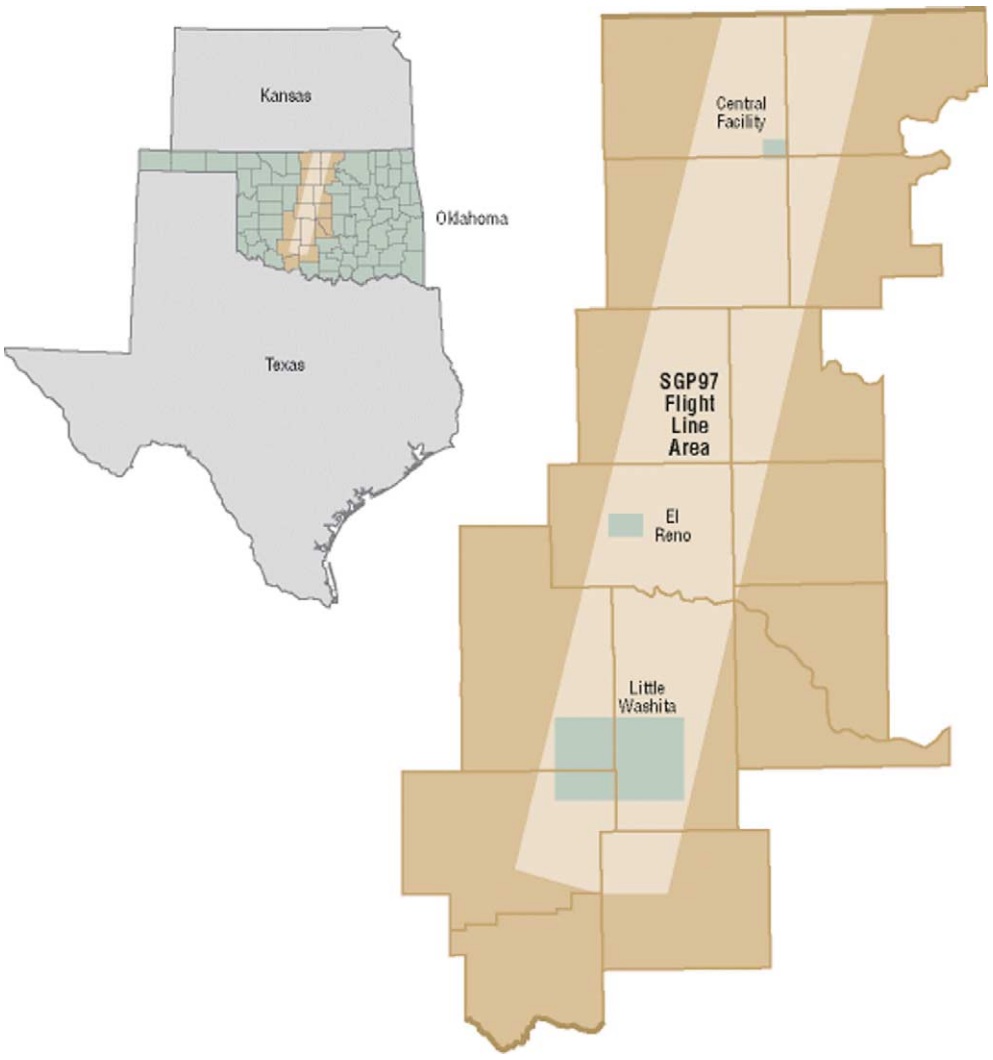

Fig. 1. General map of the Southern Great Plains, ESTAR overflight area, and ground observation sites of the SGP97 hydrology campaign.

used the same curve without any site-specific re-evaluation. Two probes were used for our measurements at each field. In situ evaluation showed no significant difference between the two probes; the analyses in the following sections are based on pooled data from both probes at each field.

4. Results and discussion

4.1. ESTAR versus theta probe data

Figs. 2, 3, and 4 show the relationship of the theta probe-measured field mean soil moisture content and the ESTAR-measured soil moisture content for LW03, LW13, and LW21, respectively. In these plots, data are shown only for the dates when both instruments were concurrently deployed. Except for one datum, the LW03 data fall around the 1:1 line, indicating a good match

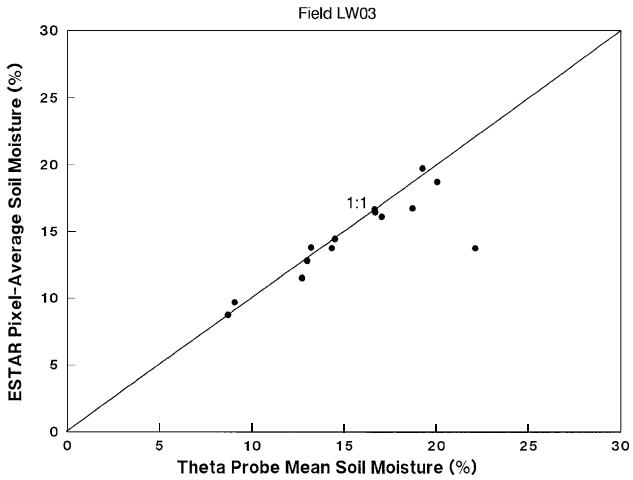

Fig. 2. Comparison of pixel-average soil moisture measured by an airborne ESTAR and mean soil moisture measured at 49 grid locations using theta probe in the LW03 pixel.

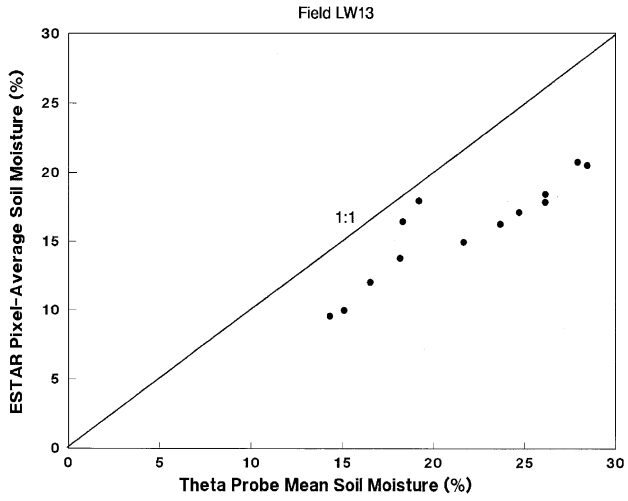

Fig. 3. Comparison of pixel-average soil moisture measured by an airborne ESTAR and mean soil moisture measured at 49 grid locations using theta probe in the LW13 pixel.

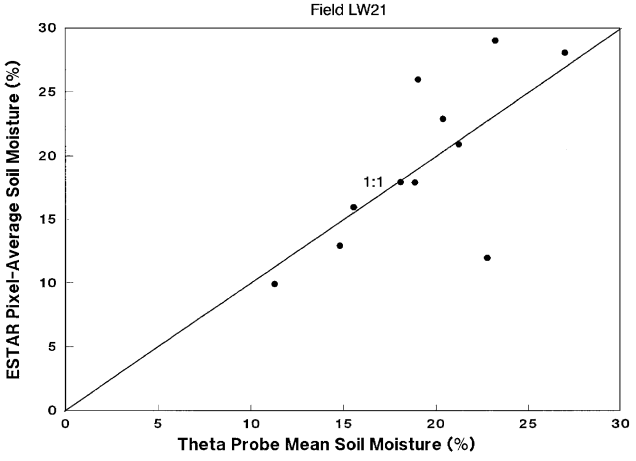

Fig. 4. Comparison of pixel-average soil moisture measured by an airborne ESTAR and mean soil moisture measured at 49 grid locations using theta probe in the LW21 pixel.

between the two instruments (Fig. 2). The LW13 data showed a systematic deviation from the 1:1 line, with ESTAR underestimating soil moisture content compared to theta probe measurements (Fig. 3). In LW21 the data again fell around the 1:1 line (Fig. 4), although the scatter was greater than observed in LW03. We attribute these differences among the pixels to characteristic combinations of soil, topography, vegetation, land management, and precipitation history, that will be discussed later.

4.2. Time-stability of ground-based observations

Following Vachaud et al. [41], we conducted a temporal stability analysis using the theta probe soil moisture measurements within each footprint. Fig. 5 shows the mean and standard deviation of the relative difference ($\delta_{i,t}$) ranked from smallest to largest. The relative difference is based on the difference ($\Delta\theta_{i,t}$) between the measured soil moisture ($\theta_{i,t}$) at location i ($i = 1, \ldots, n$) and time t ($t = 1, \ldots, T$) and the mean soil moisture ($\langle\theta\rangle_t$) at the same time. Mathematically,

$$\Delta\theta_{i,t} = \theta_{i,t} - \langle\theta\rangle_t \tag{1}$$

and

$$\langle\theta\rangle_t = \frac{1}{n}\sum_{i=1}^{n}\theta_{i,t}. \tag{2}$$

The relative difference is then defined

$$\delta_{i,t} = \frac{\Delta\theta_{i,t}}{\langle\theta\rangle_t} \tag{3}$$

and a value of $\delta_{i,t} = 0$ indicates the moisture content at the ith site is equal to the field mean on day t. Hence for any location i the time average $\langle\delta_i\rangle$, and the temporal standard deviation $\sigma(\delta_{i,t})$ can be calculated for the t observations. The advantage of this approach is that it can identify locations that systematically either overestimate ($\langle\delta_i\rangle$ higher than 0) or underestimate ($\langle\delta_i\rangle$ lower than 0) the pixel-average soil moisture. Most interestingly, it can identify the locations within a footprint that consistently monitor the mean soil moisture (with certain degrees of error) as well as the extremely wet and dry locations and the extent of their variability with respect to the pixel-mean. For example, in the LW03 pixel, 12 sites (36, 29, 7, 48, 49, 13, 15, 41, 12, 40, 30, and 18) consistently observed the pixel-mean (within $\pm 10\%$) soil moisture during the SGP97 experiment (Fig. 5). On the other hand, sites such as 14, 1, and 2 were the wettest locations with extreme variations, and sites such as 4, 31, and 37 were driest locations in the LW03 pixel.

A second approach used by Vachaud et al. [41] to examine the time-stable characteristics of soil moisture is the nonparametric Spearman rank correlation coefficient. It is defined as

$$r_S = 1 - \frac{6\sum_{i=1}^{n}(R_{i,t} - R_{i,t'})^2}{n(n^2-1)}, \tag{4}$$

where $R_{i,t}$ is the rank of the soil moisture state ($\theta_{i,t}$) observed at location i and date t and $R_{i,t'}$ is the rank at the same location, but on date t', and n is the number of observations or sampling sites ($n = 49$ in our study). A value $r_S = 1$ corresponds to identity of rank for any site, or perfect time stability between dates t and t'. In other words, the closer r_s is to 1, the more stable the process. Tables 2–4 give the computed correlation coefficients for the three footprints. The correlations are generally high for LW03 (Table 2), relatively low for LW21 (Table 4), and intermediate for LW13 (Table 3). Before discussing the causes of the observed time invariant/variant

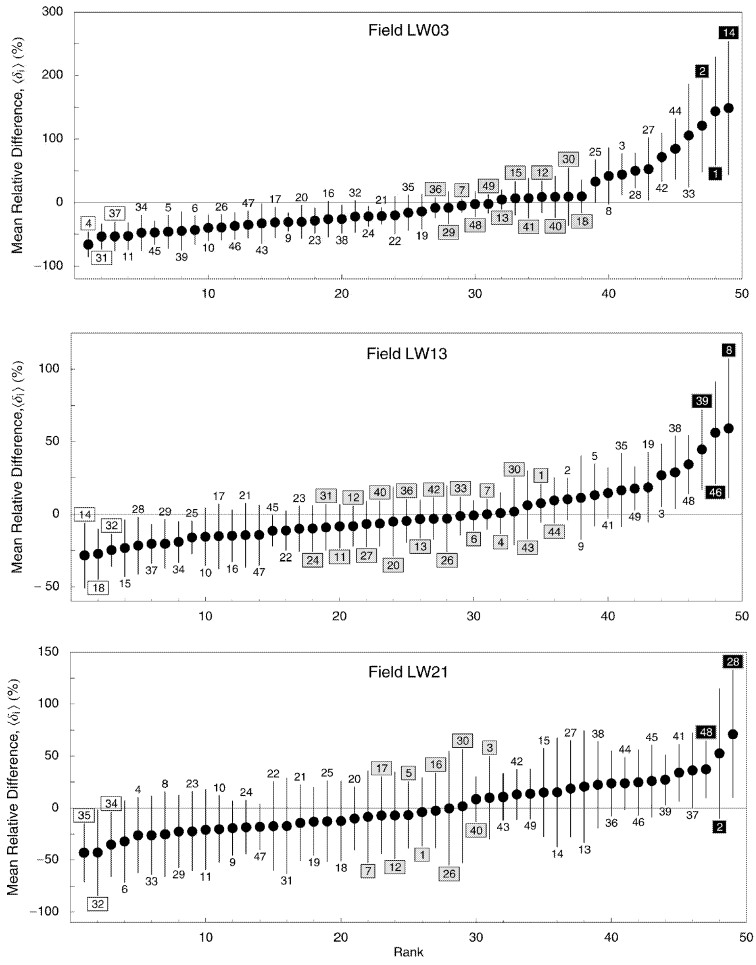

Fig. 5. Ranked intertemporal relative deviation from the mean spatial soil moisture. Vertical bars correspond to associated time standard deviation. Numbers refer to sampling grid location. The numbers surrounded by: (1) solid box indicate wettest locations, (2) shaded box indicate field-mean locations within ±10%, and (3) empty box indicate driest locations.

features of soil moisture within the footprints, we briefly review some relevant findings of previous research.

4.3. Previous studies

A key component for the understanding of the time-stable features of soil moisture involve locations encompassing various combinations of the (interactive) contributing factors, i.e., soil, topography, vegetation, and climate [6,35,38]. Among others, some of the notable data analysis studies involving these factors were made by Hills and Reynolds [20], Hawley et al. [18], Charpentier and Groffman [6], Vinnikov et al. [42], Famiglietti et al.[11], Kim and Stricker [26], Kim et al. [25], Grayson and Western [17], Western et al.[44], Western and Bloschl [43], Famiglietti et al. [13], and Mohanty et al. [28]. In the current context, we summarize the important findings of these previous soil moisture studies followed by the results of this study with relation to soil, topography, vegetation, and climate below.

Soil: Soil heterogeneity affects the distribution of soil moisture through variations in texture, organic matter content, porosity, structure and macroporosity, all of which affect the fluid transmission and retention properties. The variability in soil hydraulic conductivity and soil water retention characteristics greatly influences the vertical and lateral transmission properties. Significant soil moisture variations may exist even over very small distances due to variations in soil particle and pore sizes. Additionally, soil color influences its albedo and thus the rate of evaporative drying. In a watershed-scale study in Chicksha, OK, Hawley et al. [18] found significant differences in surface soil moisture due to differences in soil texture and antecedent moisture. From a soil-control perspective, soil moisture dynamics is related to transient upward and downward soil water fluxes. Brutsaert [4] recognized two-stages of drying of a soil profile: (1) an atmosphere-controlled stage followed by (2) a soil-controlled stage. In the first-stage, the moist soil profile can fully supply all the water demanded by the atmosphere. As the soil near the surface dries out,

Table 2
Rank correlation coefficients for field LW03

Day of year	171	172	173	175	176	177	178	179	180	181	182	183	184	186	187	188	189	190	192	194	195	197
171	1																					
172	0.91	1																				
173	0.86	0.94	1																			
175	0.75	0.8	0.74	1																		
176	0.88	0.85	0.82	0.89	1																	
177	0.82	0.76	0.65	0.86	0.9	1																
178	0.87	0.83	0.75	0.88	0.93	0.95	1															
179	0.85	0.84	0.73	0.84	0.91	0.91	0.94	1														
180	0.88	0.88	0.8	0.89	0.94	0.93	0.95	0.92	1													
182	0.91	0.85	0.8	0.86	0.93	0.9	0.94	0.91	0.95	1												
183	0.8	0.81	0.74	0.78	0.84	0.78	0.84	0.87	0.83	0.84	1											
184	0.67	0.63	0.63	0.62	0.61	0.6	0.62	0.54	0.62	0.65	0.63	1										
185	0.9	0.89	0.86	0.84	0.93	0.83	0.88	0.89	0.89	0.91	0.83	0.61	1									
186	0.75	0.76	0.69	0.7	0.76	0.73	0.77	0.83	0.8	0.81	0.8	0.51	0.84	1								
187	0.83	0.8	0.71	0.78	0.82	0.86	0.86	0.85	0.85	0.86	0.78	0.58	0.82	0.8	1							
188	0.73	0.76	0.67	0.78	0.79	0.78	0.83	0.85	0.84	0.82	0.81	0.49	0.84	0.86	0.78	1						
190	0.74	0.71	0.58	0.78	0.79	0.85	0.84	0.85	0.82	0.85	0.77	0.52	0.8	0.77	0.83	0.87	1					
192	0.76	0.76	0.65	0.73	0.74	0.83	0.84	0.81	0.82	0.79	0.73	0.63	0.74	0.69	0.8	0.75	0.81	1				
193	0.64	0.6	0.49	0.78	0.75	0.85	0.81	0.76	0.79	0.77	0.7	0.44	0.7	0.58	0.78	0.73	0.8	0.76	1			
194	0.62	0.61	0.53	0.81	0.77	0.83	0.83	0.78	0.78	0.79	0.69	0.39	0.74	0.65	0.72	0.69	0.8	0.69	0.79	1		
195	0.65	0.95	0.57	0.83	0.81	0.84	0.86	0.84	0.8	0.81	0.79	0.48	0.75	0.61	0.75	0.69	0.79	0.7	0.86	0.87	1	
196	0.7	0.69	0.59	0.82	0.82	0.85	0.85	0.85	0.82	0.83	0.75	0.45	0.8	0.7	0.75	0.83	0.88	0.74	0.78	0.84	0.84	1

Table 3
Rank correlation coefficients for field LW13

Day of year	170	171	172	173	175	176	177	178	179	180	182	183	184	185	186	187	188	190	192	193	194	195	196	197
170	1																							
171	0.88	1																						
172	0.67	0.76	1																					
173	0.73	0.8	0.62	1																				
175	0.72	0.67	0.57	0.62	1																			
176	0.81	0.78	0.67	0.71	0.8	1																		
177	0.72	0.74	0.6	0.71	0.77	0.82	1																	
178	0.36	0.47	0.5	0.44	0.4	0.48	0.46	1																
179	0.65	0.65	0.53	0.67	0.64	0.7	0.72	0.46	1															
180	0.61	0.6	0.47	0.64	0.71	0.76	0.78	0.38	0.69	1														
182	0.6	0.59	0.51	0.62	0.72	0.81	0.74	0.53	0.72	0.78	1													
183	0.45	0.66	0.5	0.58	0.51	0.59	0.54	0.56	0.5	0.52	1													
184	0.71	0.66	0.51	0.57	0.6	0.7	0.68	0.37	0.63	0.66	0.58	0.53	1											
185	0.36	0.44	0.44	0.23	0.55	0.4	0.43	0.2	0.42	0.36	0.4	0.44	0.42	1										
186	0.63	0.67	0.58	0.55	0.68	0.73	0.77	0.48	0.72	0.68	0.75	0.62	0.62	0.5	1									
187	0.65	0.58	0.39	0.54	0.51	0.62	0.57	0.22	0.44	0.46	0.51	0.33	0.66	0.36	0.46	1								
188	0.72	0.78	0.66	0.6	0.62	0.7	0.66	0.38	0.53	0.58	0.54	0.63	0.66	0.54	0.62	0.61	1							
190	0.5	0.55	0.42	0.39	0.59	0.57	0.55	0.36	0.59	0.5	0.58	0.62	0.54	0.57	0.62	0.44	0.54	1						
192	0.33	0.3	0.19	0.23	0.23	0.25	0.28	0.1	0.32	0.24	0.36	0.14	0.38	0.35	0.46	0.41	0.28	0.45	1					
193	0.51	0.47	0.27	0.33	0.43	0.45	0.39	0.45	0.44	0.49	0.24	0.44	0.44	0.33	0.5	0.53	0.37	0.37	0.59	1				
194	0.47	0.48	0.41	0.44	0.32	0.39	0.42	0.31	0.39	0.42	0.37	0.27	0.44	0.24	0.56	0.5	0.43	0.32	0.66	0.65	1			
195	0.54	0.51	0.27	0.31	0.51	0.47	0.51	0.4	0.36	0.36	0.46	0.38	0.39	0.42	0.49	0.52	0.47	0.41	0.4	0.68	0.53	1		
196	0.52	0.55	0.5	0.47	0.43	0.53	0.55	0.57	0.5	0.39	0.56	0.48	0.47	0.41	0.56	0.51	0.52	0.47	0.33	0.63	0.5	0.62	0.1	
197	0.59	0.67	0.55	0.5	0.54	0.53	0.5	0.45	0.48	0.3	0.56	0.58	0.42	0.43	0.55	0.58	0.62	0.5	0.42	0.53	0.46	0.6	0.66	1

Table 4
Rank correlation coefficients for field LW21

Day of year	173	175	177	179	180	181	182	183	184	187	188	189	192	193	194	195	197
173	1																
175	0.42	1															
177	0.4	0.46	1														
179	0.09	0.27	−0.08	1													
180	0.14	0.4	0.19	0.23	1												
181	0.08	0.26	−0.04	0.5	0.28	1											
182	0.07	0.03	−0.25	0.21	0.22	0.38	1										
183	0.09	0.23	0.09	0.16	0.35	0.41	0.33	1									
184	0.03	0.15	0.05	0.27	0.3	0.34	0.43	0.38	1								
187	0.17	0.04	−0.03	0.08	0.31	0.38	0.25	0.34	0.29	1							
188	−0.06	0.12	−0.12	0.26	0.13	0.28	0.31	0.4	0.28	0.29	1						
189	0.14	0.26	0.04	0.38	0.4	0.46	0.4	0.31	0.54	0.22	0.26	1					
192	0.07	−0.02	−0.08	0.38	0.27	0.34	0.65	0.42	0.38	0.26	0.38	0.48	1				
193	0.13	0.01	−0.19	0.3	0.24	0.44	0.71	0.36	0.49	0.21	0.32	0.51	0.69	1			
194	0.17	0.16	−0.16	0.5	0.32	0.53	0.58	0.4	0.45	0.23	0.33	0.73	0.58	0.64	1		
195	0.03	−0.01	−0.17	0.14	0.24	0.41	0.57	0.37	0.37	0.41	0.44	0.42	0.6	0.65	0.46	1	
197	0	0.03	−0.25	0.42	0.17	0.53	0.61	0.49	0.51	0.36	0.43	0.51	0.67	0.67	0.7	0.58	1

moisture can no longer be delivered at the rate demanded by the atmosphere. Instead, the moisture delivery rate is limited by the properties of soil profile. Brutsaert [4] notes that at any one point, the transition from atmosphere to soil control is rapid, but over the entire catchment the change over will be gradual. Famiglietti et al. [11] demonstrated some of these concepts related to soil heterogeneity and consequential flux rates using a distributed catchment-scale water balance model.

Entekhabi [9] presented a sensitivity analysis of influence of soil texture on land-atmosphere interaction and pointed out the complex nature of the relationship. More recently, Kim et al. [25] showed the impact of soil heterogeneity on the water budget of the unsaturated zone. They showed that in highly conductive soils, where evapotranspiration is limited by percolation through a lower boundary, heterogeneity increases the spatially average evapotranspiration relative to the uniform soil. For less conductive soils, decreasing infiltration rates due to soil heterogeneity cause evapotranspiration to become smaller. They also concluded that equivalent parameters derived for the long-term average water budget are not valid for transient behavior and depend not only on the soil hydraulic parameters and their heterogeneity but also on the climate and the spatially uniform parameters. In a related study, Kim and Stricker [26] showed the stronger effect of soil spatial heterogeneity on components of the water budget for a loamy soil as compared to a sandy soil. They suggested that soil heterogeneity has a great influence for the loamy soil because most of the variation of the water budget is present at the smaller (field) scale. On the other hand, most of the water budget variation for the sandy soil, occurs at larger scales and is temporally correlated to the rainfall field. These findings led them to conclude that from the perspective of annual water budget a homogenous equivalent soil exists for the sandy soil but not for the loamy soil. Some of the other significant studies of soil moisture variability in relation to different soil properties were made by Reynolds [35], Henninger et al. [19], Niemann and Edgell [32], Crave and Gascuel-Odoux [8], and Famiglietti et al. [12].

Topography: Topography also plays an important role in the spatial organization of soil moisture at different scales. Variations in slope, aspect, curvature, upslope contributing area, and relative elevation all affect the distribution of soil moisture near the land surface. At the small catchment and hillslope scales, soil moisture varies as a result of water-routing processes, radiative (aspect) effects, and heterogeneity in vegetation and soil characteristics. Hills and Reynolds [20] conducted an extensive study and attempted to relate slope and soil moisture on hillslope areas. They found some patterns but felt that the interaction of other factors made it impossible to develop a deterministic relationship. On the contrary, Hawley et al. [18] found that topography was the most significant factor controlling the distribution of soil moisture within the small agricultural watersheds at Chicksha, OK. Charpentier and Groffman [6] studied the effects of topography and moisture content on the variability of soil moisture within remote sensing pixels during the First ISLSCP field experiment (FIFE). They showed that within-pixel (66 m $\times$ 66 m) soil moisture variability increased with increased topographic heterogeneity. A flat pixel had significantly lower standard deviations and fewer outlier points than a sloping or a valley pixel. Furthermore, they observed that remote sensing reflected soil moisture conditions less accurately on pixels with increased topographic variability and less precisely when soil is dry. More recently, Mohanty et al. [28] showed the dominance of a slope-effect on the diurnal soil moisture distribution in a gentle slope during the SGP97 Hydrology Experiment. Several other studies also showed that location on the slope is very important in determining soil moisture variation, suggesting that a simple averaging of soil moisture values over the slope may lead to errors at different timescales. In Australia, Western et al. [44] showed partial area saturation excess runoff to be an important runoff-producing process in many catchments. This runoff is believed to be associated with systematic or organized spatial variation in soil moisture, particularly saturated areas associated with topographic convergence.

Besides overland flow, subsurface flows play a very important role in the redistribution of soil moisture between storm events [11,28]. For areas of relatively shallow soil the local topography exerts a dominant control on these subsurface flows. In particular, areas of higher antecedent wetness, which have a greater likelihood of generating runoff and evaporation at the potential rate, should be expected in areas of convergent flow in plan and concave slopes in profile. These areas are commonly found in hillslope hollows and above the heads of the smallest (first-order) stream channels. With several illustrative examples, Grayson et al. [16] further suggested the characteristic local control (dominance of vertical over lateral water fluxes due to soil properties and local terrain) during dry condition and nonlocal control (dominant lateral surface and subsurface water flux due to catchment terrain) during wet conditions govern the soil moisture spatial patterns. Entekhabi and Rodriguez-Itrube [10] analyzed the space and timescales of variability in the soil moisture field and identified the key roles of topography and precipitation variability in defining its statistical characteristics. Other studies relating soil moisture variability and topography were made by Reid [34], Hawley et al. [18], Moore et al. [30], Loague [27], Niemann and Edgell [32], Crave and Gasuel-Odoux [8], and Famiglietti et al. [12].

Vegetation: Land cover is also critical for understanding the soil moisture regimes as it affects infiltration, runoff, and evapotranspiration. Vegetation type, density, and uniformity are some of the associated features that contribute to soil moisture variation at different space and timescales [35]. Furthermore the influence of vegetation on soil moisture is more dynamic as compared to soil and topographic factors. Literature shows that the variability of soil moisture is lowest with full canopy cover and highest with partial coverage. Hawley et al. [18] demonstrated that various vegetation–topography–soil combinations lead to temporal persistence (clustering) of soil moisture patterns in complex terrains with mixed vegetation. They also suggested that the presence of vegetation tends to diminish the soil moisture variations caused by topography. Vinnikov et al. [42] noticed differences in soil moisture evolution for three catchments at Valdai, Russia with different vegetation. More recently, Mohanty et al. [29] showed the evolution of the soil moisture spatial structure in a mixed-vegetation remote-sensing footprint (LW21) during the SGP97 field campaign. Their results showed

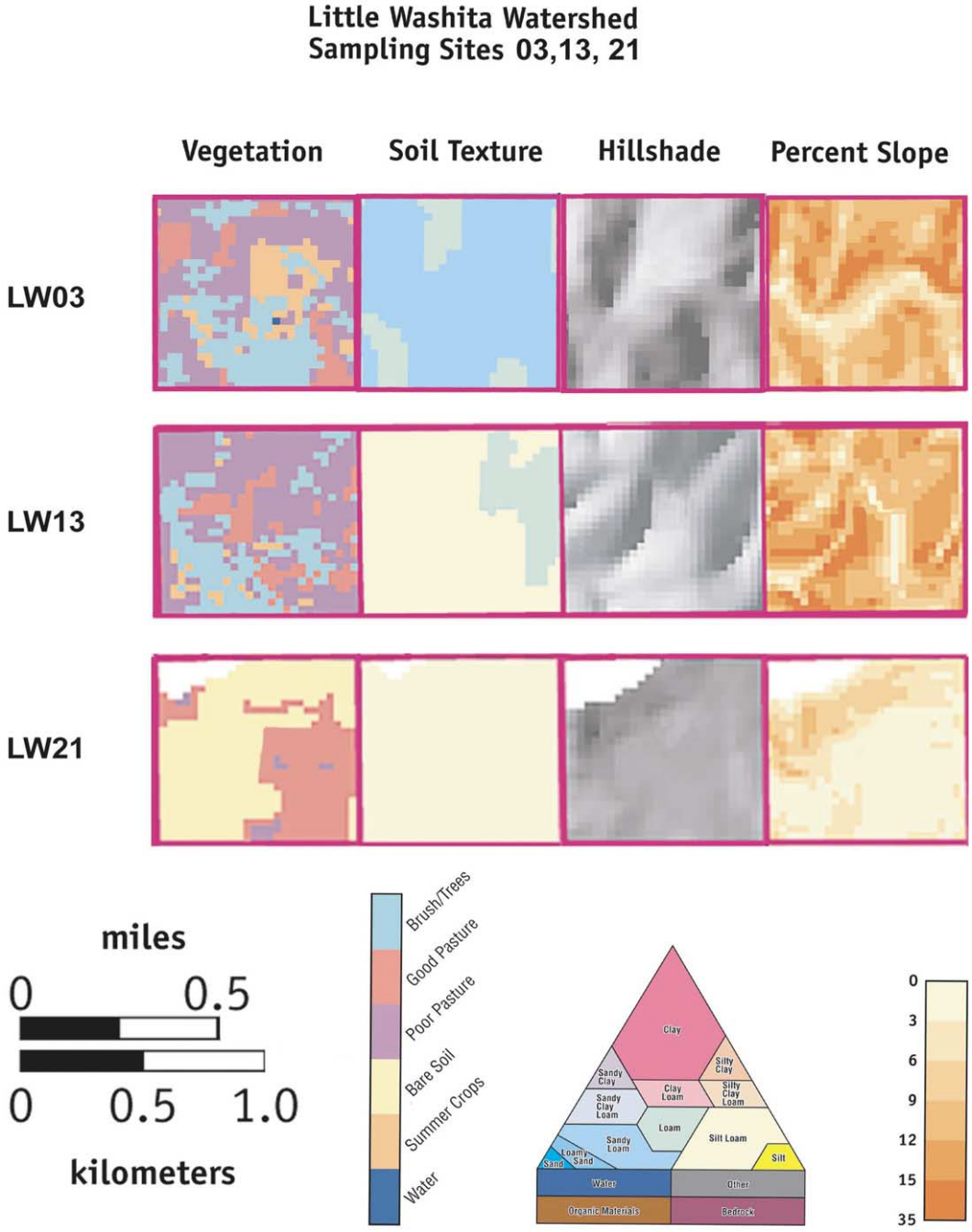

Fig. 6. Characteristic land surface attributes (soil texture, percent slope, hillshade, and vegetation type) for the LW03, LW13, and LW21 pixel.

that the vegetation dynamics (growth/decay), land management (tillage), and precipitation events controlled the intra-seasonal soil moisture spatial structure for the pixel with flat topography and uniform soil texture.

Climate: Precipitation, solar radiation, wind, and humidity are some of the important climatic factors that contribute to the space–time dynamics of soil moisture. Precipitation is the single most important climatic forcing for soil moisture content and its distribution. Some of the earlier studies showed that the level of soil moisture variation increases with moisture content and rainfall, and decreases with isolation and time since the last rainfall. In other words, as the system moves toward equilibrium, it becomes more homogeneous, with soil moisture being less variable at higher tensions than near saturation. However, there may be an increase in variation under extremely dry conditions. Bell et al. [3] analyzed soil moisture variability under various climatic conditions while other extrinsic factors (soil texture, vegetation, land management, and topographic conditions) were more or less similar. As shown by Sivapalan et al. [39], the dominant runoff producing mechanism may vary with storm characteristics and antecedent conditions resulting spatio-temporal variability in soil moisture. During the SGP97 hydrology campaign, Famiglietti et al. [13] found a distinct trend in mean soil moisture for Little Washita (in southern Oklahoma), El Reno (in central Oklahoma), and DOE-ARM Central Facility (in north Oklahoma) locations with a south-to-north precipitation gradient.

4.4. SGP97: sub-pixel soil moisture variability and causes

While all these previous research findings describe the sources and nature of soil moisture variation, the relative importance of these causative factors is yet to be evaluated fully under different hydrologic scenarios and space–time scales. In this study we made soil moisture measurements encompassing different soil–topography–vegetation–climate combinations at the 100 m × 100 m grid-scale (ground measurements) and 800 m × 800 m footprint-scale which can subsequently be used to derive (non)linear relationships of hydrologic processes (or properties) dominant at these scales. Fig. 6 shows characteristic soil–topography–vegetation features, including soil texture (based on the county soil survey map), slope (based on the USGS digital elevation map), and vegetation (based on NASA Landsat Thematic

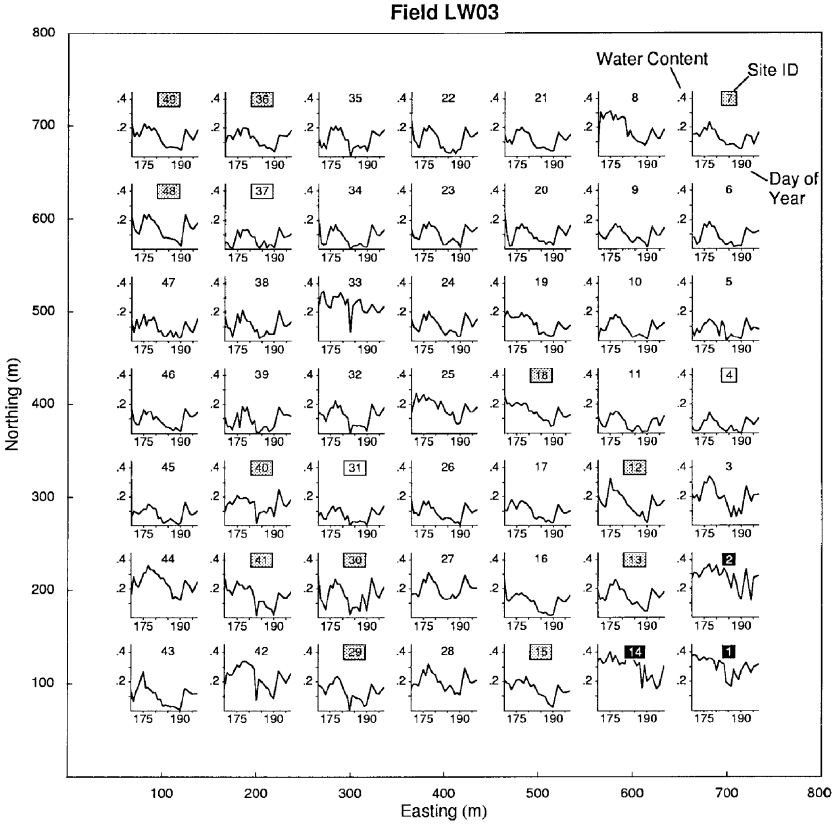

Fig. 7. Spatio-temporal evolution plot of soil moisture in a regular 7 × 7 grid across the LW03 pixel (800 m × 800 m) during SGP97 hydrology campaign. The numbers surrounded by: (1) solid box indicate wettest locations, (2) shaded box indicate field-mean locations within ±10%, and (3) empty box indicate driest locations based on temporal stability analysis.

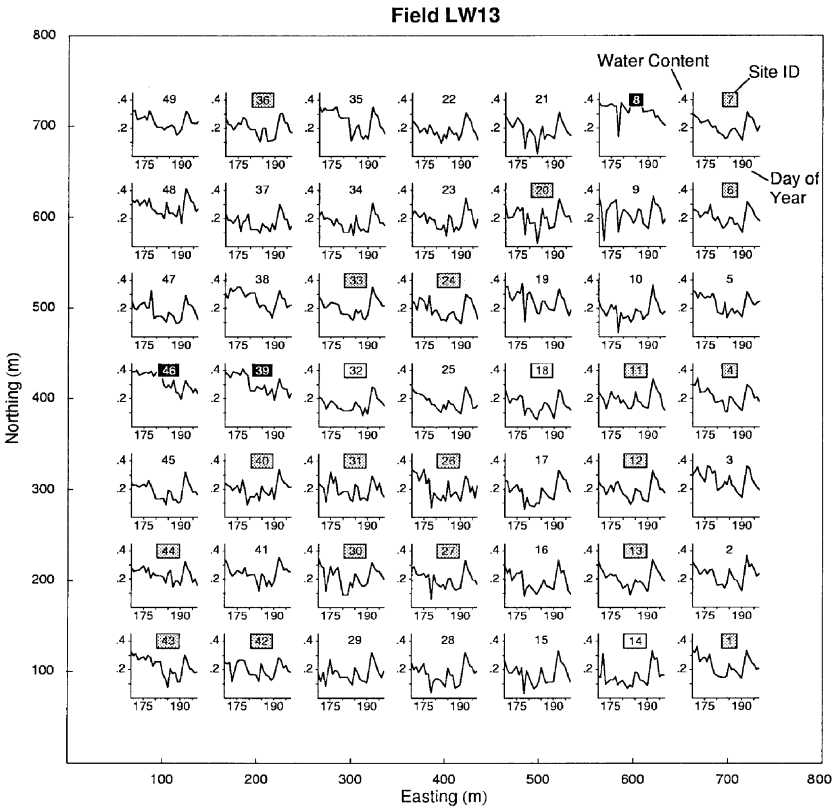

Fig. 8. Spatio-temporal evolution plot of soil moisture in a regular 7×7 grid across the LW13 pixel (800 m $\times$ 800 m) during SGP97 hydrology campaign. The numbers surrounded by: (1) solid box indicate wettest locations, (2) shaded box indicate field-mean locations.28 within $\pm 10\%$, and (3) empty box indicate driest locations based on temporal stability analysis.

Mapper (TM) imagery made during the SGP97 experiment) for the three selected remote sensing footprints. Correspondingly, Figs. 7–9 show the soil moisture evolution at 49 grid node locations within each foot print during the SGP97 experiment. In these soil moisture plots, any break in daily sampling was filled by a straight line between the dates. These spatio-temporal evolution plots demonstrate that each sampling site within a remote sensing footprint has a unique characteristic trend based on associated soil, slope, and vegetation properties. Figs. 7–9 also show the location of mean and extreme (wet or dry) sites that were identified in the temporal stability analysis (Fig. 5). Overall, LW03 showed the best time-stable features (i.e., $\langle \delta \rangle_i \approx 0$ and small temporal standard deviation $\sigma(\delta_{i,t})$) at several sampling locations (within $\pm 10\%$). Additionally, as noted previously, the rank correlation coefficients between sampling dates were generally high for LW03 (Table 2). Another notable feature in LW03 was that the wettest sites showed higher temporal standard deviation $(\sigma(\delta_{i,t}))$ than the drier sites. For the LW13 field, several locations observed time-stable mean characteristics. But note that some of these sites were subject to large temporal standard deviations $(\sigma(\delta_{i,t}))$. The LW21 pixel showed the worst time stable features among the three pixels. The sampling sites which fell close to the mean relative difference (i.e., $\langle \delta_i \rangle = 0$) were subject to large temporal variations $(\sigma(\delta_{i,t}))$, although some of the drier or wetter sites had relatively small temporal variations. Thus, judging the sites with true temporal stability was difficult in this case. Again, these findings are corroborated by the rank correlation coefficients for the three pixels, with the highest being found for LW03 (Table 1) and the lowest for LW21 (Table 3).

In summary, among the three pixels, the sandy loam soil with gently rolling topography and range land cover (LW03) produced the best time-stable soil moisture pattern. The silty loam soil with gently rolling topography and range land cover (LW13) produced an intermediate level of time-stability, and the silty loam soil with flat topography and a split winter wheat/grass land cover (LW21) generated the least time-stable phenomena. We suggest that these characteristic surface features, along with precipitation patterns for the three pixels, are possible reasons for the different degrees of agreement between the ESTAR (pixel-average) soil moisture measurements and the distributed ground sampling (Figs. 1–3). This may indicate that the remote sensing soil moisture measurements need improved calibration algorithms for footprints with varying degrees of complexity in terms of soil, slope, and vegetation combinations.

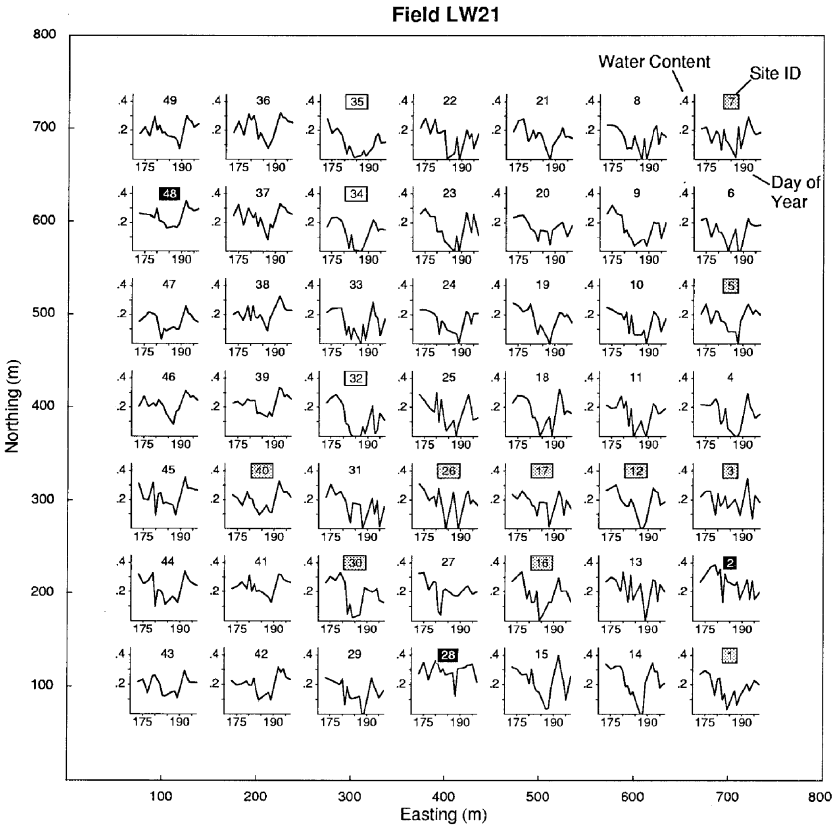

Fig. 9. Spatio-temporal evolution plot of soil moisture in a regular 7×7 grid across the LW21 pixel (800 m $\times$ 800 m) during SGP97 hydrology campaign. The numbers surrounded by:(1) solid box indicate wettest locations, (2) shaded box indicate field-mean locations within $\pm 10\%$, and (3) empty box indicate driest locations based on temporal stability analysis.

Overlaying the pixel-scale space–time soil moisture evolution maps (Figs. 7–9) on the soil texture, slope, hillshade, and vegetation maps (Fig. 6) for the three pixels revealed some interesting correlations. Note, however, that most of these interpretations are qualitative and done in an exploratory sense. The accuracy and precision of the attribute maps (soil texture, slope, vegetation) are a reasonable match to our soil moisture sampling grid, although a few concerns still exist. For example, the vegetation maps are based on limited Landsat TM snap shots, with their temporal dynamics and interpretation being adjudged by visual observation during the SGP97 campaign.

For the LW03 pixel, most of the sampling sites with time-stable mean soil moisture signal (within $\pm 10\%$) were clustered on the southern side of the pixel following a medium slope contour and brush/tree vegetation patch. Another cluster of sites on the north-west corner of the pixel showed the mean signal dominated by mixed pasture and more variable slope. The three wettest spots (with large temporal variation) for the LW03 pixel were located on the south-east corner characterized by good pasture and smaller slope, whereas the three driest spots were distributed across the pixel and lie on steeper slopes and poor pasture. On the contrary, in the LW13 pixel, time-stable soil moisture within $\pm 10\%$ of the field mean were observed in multiple clusters. We did not find any consistent characteristics in terms of soil, slope, or vegetation individually for these mean clusters. However, certain characteristic combinations of these factors are probably responsible for this behavior. The three wettest and three driest spots of the pixel were located on medium slope with no visible correspondence with vegetation. Soil texture is the major difference between LW03 and LW13 pixels while vegetation (pasture), topography (rolling), and precipitation (Fig. 4, Famiglietti et al. [13]) are more or less similar. Based on the above findings we suggest that the silty loam soil (LW13) is more variable in terms of space–time dynamics of soil moisture processes as compared to the sandy loam soil (LW03). This reasoning may somewhat explain the systematic errors incurred by the ESTAR remote sensor in LW13. In the LW21 pixel, soil texture (silty loam) and slope (flat) are uniform, and vegetation and precipitation dominate the spatio-temporal distribution of soil moisture. Because land cover and land management (tillage of the winter wheat field) is more dynamic, less time-stability was observed in this case. Research on developing quanti-

tative (non)linear relationships between soil moisture and various soil (e.g., texture, hydraulic conductivity, soil water retention), topography (e.g., slope, aspect, relative elevation, upslope contributing area), and vegetation (e.g., type, canopy density, root density, LAI) characteristics within these remote sensing footprints is ongoing and will be published at a later date. Furthermore, geostatistical analysis of these data sets may reveal deterministic relationships between the correlation structures of ground-based soil moisture contents and footprint-scale average soil moisture measured by ESTAR.

5. Conclusions

Based on our analysis of ground and remote sensing soil moisture data, the following conclusions were drawn:

1. Characteristic differences were observed in the space–time dynamics of soil moisture within selected footprints with various combinations of soil texture, slope, vegetation, and precipitation.
2. Better time-stable features were observed within a footprint, containing sandy loam soil (LW03) than was observed in footprints containing silt loam soil (LW13 and LW21).
3. Flat topography with split wheat/grass land cover (LW21) resulted the largest spatio-temporal variability and the least time-stability in soil moisture.
4. ESTAR footprint-average soil moisture was well calibrated for the LW03 pixel with sandy loam soil, rolling topography, and pasture land cover, but improved calibration is warranted for the LW13 (silty loam soil, rolling topography, pasture land) and LW21 (silty loam soil, flat topography, split vegetation of wheat and grass land with tillage practice) pixels.

Acknowledgements

The help of many SGP97 participants in the field data collection is acknowledged. This study was funded by NASA Land Surface Hydrology Program grant # NAG5-8682 and NSF-SAHRA at the University of Arizona.

References

[1] Allen PB, Naney JW. Hydrology of the Little Washita river watershed, Oklahoma: data and analyses. USDA-ARS, ARS-90, Washington, DC, 1991, 74 pp.
[2] Arya LM, Paris JF. A physical model to predict the soil moisture characteristic from particle size distribution and bulk density. Soil Sci Soc Am J 1981;45:1023–30.
[3] Bell KR, Blanchard BJ, Schmugge TJ, Witczak MW. Analysis of surface moisture variations within large field sites. Water Resour Res 1980;16:796–810.
[4] Brutsaert W, Evaporation into the atmosphere. Reidel, Norwell, MA, 1982, 299 p.
[5] Carsel RF, Parrish RS. Developing joint probability distributions of soil water retention characteristics. Water Resour Res 1988;24:755–69.
[6] Charpentier MA, Groffman PM. Soil moisture variability within remote sensing pixels. J Geophys Res 1992;97:18987–95.
[7] Cosby BJ, Hornberger GM, Clapp RB, Ginn TR. A statistical exploration of the relationships of soil moisture characteristics to the physical properties of soils. Water Resour Res 1984;20:682–90.
[8] Crave A, Gascuel-Odoux C. The influence of topography on time and space distribution of soil surface water content. Hydrolog Processes 1997;11:203–10.
[9] Entekhabi D. A simple model of the hydrologic cycle and climate: 1. Model construct and sensitivity to the land surface boundary. Adv Water Resour 1994;17:79–91.
[10] Entekhabi D, Rodriguez-Itrube I. Analytical framework for the characterization of the space–time variability of soil moisture. Adv Water Resour 1994;17:35–45.
[11] Famiglietti JS, Wood EF, Sivapalan M, Thongs DJ. A catchment scale water balance model for FIFE. J Geophys Res 1992;97(D17):18997–9007.
[12] Famiglietti JS, Rudnicki JW, Rodell M. Variability in surface moisture content along a hillslope transect: Rattlesnake hill, TX. J Hydrol 1998;210:259–81.
[13] Famiglietti JS, Devereaux JA, Laymon CA, Tsegaye T, Houser PR, Jackson TJ, et al. Ground-based investigation of soil moisture variability within remote sensing footprints during the Southern Great Plains (1997) Hydrology Experiment. Water Resour Res 1999;35:1839–51.
[14] Gaskin GJ, Miller JD. Measurement of soil water content using a simplified impedance measuring technique. J Ag Eng Res 1996;63:153–60.
[15] Georgakakos KP, editor. Soil moisture theories and observations. J Hydrol 1996;184:1–152.
[16] Grayson RB, Western AW, Chiew FHS. Preferred states in spatial soil moisture patterns: Local and nonlocal controls. Water Resour Res 1997;33:2897–908.
[17] Grayson RB, Western AW. Towards areal estimation of soil water content from point measurements: time and space stability of mean response. J Hydrol 1998;207:68–82.
[18] Hawley ME, Jackson TJ, McCuen RH. Surface soil moisture variation on small agricultural watersheds. J Hydrol 1983;62:179–200.
[19] Henninger DL, Petersen GW, Engman ET. Surface soil moisture within a watershed-variations, factors influencing, and relationship to surface runoff. Soil Sci Soc Am J 1976;40:773–6.
[20] Hills TC, Reynolds SG. Illustrations of soil moisture variability in selected areas and plots of different sizes. J Hydrol 1969;8:27–47.
[21] Jackson TJ, Le Vine DE. Mapping surface soil moisture using an aircraft-based passive microwave instrument: algorithm and example. J Hydrol 1996;184:85–99.
[22] Jackson TJ, Schiebe FR, editors. Washita' 92 data report, NAWQL report 101, USDA National Agricultural Water Quality Laboratory, Durant, OK, 1993.
[23] Kachanoski RG, de Jong E. Scale dependence and the temporal persistence of spatial patterns of soil water storage. Water Resour Res 1988;24:85–91.
[24] Kamgar A, Hopmans JW, Wallender WW, Wendroth O. Plotsize and sample number for neutron probe measurements in small field trials. Soil Sci 1993;156(4):213–24.
[25] Kim CP, Stricker JNM, Feddes RA. Impact of soil heterogeneity on the water budget of the unsaturated zone. Water Resour Res 1997;33:991–9.

[26] Kim CP, Stricker JNM. Influence of variable soil hydraulic properties and rainfall intensity on the water budget. Water Resour Res 1996;32:1699–712.
[27] Loague K. Soil water content at R-5. Part-1. Spatial and temporal variability. J Hydrol 1992;139:233–51.
[28] Mohanty BP, Skaggs TH, Famiglietti JS. Analysis and mapping of field-scale soil moisture variability using high-resolution ground based data during the Southern Great Plains 1997 (SGP97) Hydrology Experiment. Water Resour Res 2000;36: 1023–32.
[29] Mohanty BP, Famiglietti JS, Skaggs TH. Evolution of soil moisture spatial structure in a mixed vegetation pixel during the Southern Great Plains 1997 (SGP97) Hydrology Experiment. Water Resour Res 2000;36:3675–86.
[30] Moore ID, Burch GJ, Mackenzie DH. Topographic effects on the distribution of surface water and the location of ephemeral gullies. Trans ASAE 1988;31:1098–107.
[31] National Research Council, Opportunities in hydrologic sciences, National Academy Press, Washington, DC, 1991; 348 pp.
[32] Niemann KO, Edgell CR. Preliminary analysis of spatial and temporal distribution of soil moisture on a deforested slope. Phys Geography 1993;14:449–64.
[33] Njoku EG, Entekhabi D. Passive microwave remote sensing of soil moisture. J Hydrol 1996;184:101–29.
[34] Reid I. The influence of slope orientation upon the soil moisture regime and its hydromorphological significance. J Hydrol 1973;19:309–21.
[35] Reynolds SG. The gravimetric method of soil moisture determination, part III: an examination of factors influencing soil moisture variability. J Hydrol 1970;11:288–300.
[36] Schaap MG, Leij FJ, van Genuchten MT. Neural network analysis for hierarchical prediction of soil hydraulic properties. Soil Sci Soc Am J 1998;62:847–55.
[37] Schmugge T. Applications of passive microwave observations of surface soil moisture. J Hydrol 1998;212–213:188–97.
[38] Sharma ML, Luxmoore RJ. Soil spatial variability and its consequences on simulated water balance. Water Resour Res 1979;15:1567–73.
[39] Sivapalan M, Beven K, Wood EF. On hydrologic similarity 2. A scaled model of storm runoff production. Water Resour Res 1987;23:2266–78.
[40] Stewart JB, Engman ET, Feddes RA, Kerr Y, editors. Scaling up in hydrology using remote sensing. Chichester: Wiley; 1996, 255 p.
[41] Vachaud G, De Silans AP, Balabanis P, Vauclin M. Temporal stability of spatially measured soil water probability density function. Soil Sci Soc Am J 1985;49:822–8.
[42] Vinnikov KY, Robock A, Speranskaya N, Schlosser CA. Scales of temporal and spatial variability of midlatitude soil moisture. J Geophys Res 1996;101:7163–74.
[43] Western AW, Bloschl G. On the spatial scaling of soil moisture. J Hydrol 1999;217:203–24.
[44] Western AW, Grayson RB, Bloschl G, Willgoose GR, McMahon TA. Observed spatial organization of soil moisture and its relation to terrain indices. Water Resour Res 1999;35:797–810.